UCLA
UCLA Previously Published Works

Title

Virtually Constrained Admittance Control using Feedback Linearization for Physical Human-Robot Interaction with Rehabilitation Exoskeletons

Permalink

Authors

Sun, Jianwei
Foroutani, Yasamin
Rosen, Jacob

Publication Date

DOI

Supplemental Material

Peer reviewed

Virtually Constrained Admittance Control using Feedback Linearization for Physical Human-Robot Interaction with Rehabilitation Exoskeletons

Jianwei Sun[1], Yasamin Foroutani[1], and Jacob Rosen[1]

Abstract—Robot-assisted rehabilitation focuses in part on path-based assist-as-needed reaching rehabilitation, which dynamically adapts the level of robot assistance during physical therapy to ensure patient progress along a predefined trajectory without over-reliance on the system. Additionally, bimanual exoskeletons have enabled asymmetric rehabilitation schemes, which leverage the patient's healthy side to guide the rehabilitation through interactions with objects in virtual reality that replicate activities of daily living. Within the context of physical human-robot interaction, these tasks can be formulated as constraints on the space of allowable motions. This study introduces a novel feedback linearization-inspired time-invariant admittance control scheme that enforces these motion constraints by isolating and stabilizing the component of the virtual dynamics transversal to the constraint. The methodology is applied to two rehabilitation tasks: (1) a path-guided reaching task with restoring force field, and (2) a bimanual interaction with a virtual object. Each task is then evaluated on one of two drastically different exoskeleton systems: (1) the V-Rex, a non-anthropomorphic full-body haptic device, and (2) the EXO-UL8, an anthropomorphic bimanual upper-limb exoskeleton. The two systems exist on opposite ends of the task/joint space control, non-redundant/redundant, off-the-shelf (industrial)/custom, non-anthropomorphic/anthropomorphic spectra. Experimental results validate and support the methodology as a generalizable approach to enabling constrained admittance control for rehabilitation robots.

Index Terms—Physical human-robot interaction (pHRI), admittance control, feedback linearization, holonomic constraints, rehabilitation exoskeletons

I. INTRODUCTION

The field of robot-assisted rehabilitation in the context of *physical human-robot interaction* (pHRI) has experienced a recent surge in attention [1]–[4] in areas focused on improving rehabilitation effectiveness and safety. One such instance is path-guided rehabilitation, where the robot guides a patient through a desired trajectory and often implements *assist-as-needed* (AAN) schemes that adapt the level of robot assistance to ensure progress without fostering over-reliance. Another instance is the development of bimanual exoskeletons, which has enabled asymmetric rehabilitation schemes that leverage the patient's healthy side to guide the rehabilitation through *virtual reality* (VR)-based training tasks that replicate *activities of daily living*s (ADLs) [5], [6]. These two categories of rehabilitation tasks motivate and structure our contribution.

In path-guided robot-assisted rehabilitation, guidance virtual fixtures [7]–[10], virtual force fields, and force fields with saturation [11]–[13] are often used to guide motion towards predefined paths. The restoring force can be generated by virtual springs [14], [15], spring damper systems [16], or viscoelastic couplings [17]. A limitation of these approaches is that the robot's physical and virtual dynamics are often neglected, which are influenced by the force fields and impact guidance performance. To this end, velocity-field trajectories, where the path is defined as a velocity profile, have been explored in conjunction with adjustable deadzones and adaptive learning strategies [18], [19]. However, all the aforementioned approaches are limited by requiring explicit consideration of the path's geometry in the force or velocity field definition and stability assessment. This ultimately limits their generalizability to new paths, which exists in abundance in ADLs.

Since many ADLs are bimanual [6], [20], robot-assisted rehabilitation has also explored bimanual rehabilitation, which is primarily facilitated through bimanual exoskeletons [1], [6], [21]–[23], and often synergistically integrated with immersive VR environments [2], [3], [24]. These training schemes can emulate haptic interaction with virtual objects, which is known to be an important aspect of the motor learning process when used in conjunction with visual feedback [25], [26]. However, a challenge of creating stable interaction is rendering stiff objects, which requires large forces to be generated from small displacements [6], [27]. Hybrid force-position control has also been studied [28], [29], but the complexity of impedance control may not be necessary for applications that are more concerned about spatial accuracy. Advanced simulation tools, such as [30], [31], require the exact geometry of the virtual object, making implementation highly dependent on the object. Furthermore, convex approximations may be needed to accurately compute interaction forces, limiting accuracy for complex geometries. These problems are inherent to dynamics-based approaches, even though the end objective may only be concerned about the kinematics of the interaction.

In either path-based reaching tasks or bimanual interaction with virtual rigid objects, the robot's motions must be restricted to a subset. For the former, the subset is a predefined path. For the latter, the subset is the space of motions in which the relative pose of the hands is constant. Subset stabilization has been explored through transverse feedback linearization, which decouples the system dynamics into tangential and transversal subsystems relative to the subset [32], [33], and has found application in constrained pHRI [34]. While the decoupled dynamics can simplify the design of feedback controllers, such techniques require local coordinates for both subsystems, which can be difficult to find in general (e.g., for the desired motion subset in bimanual interaction).

---
[1]The authors are with the Department of Mechanical and Aerospace Engineering at the University of California, Los Angeles (UCLA), USA 90095. {sunjianw1, yforoutani, jacobrosen}@ucla.edu

We present a novel feedback linearization-inspired admittance control methodology for holonomically constrained pHRI. Specifically, we model the desired motion constraint as a submanifold and apply feedback linearization to isolate the motion component transversal to the constraint, without requiring local coordinates for the tangential component. Our approach unifies the two discussed motion constraints prevalent in robot-assisted rehabilitation. It overcomes the aforementioned challenges in path-based reaching by decoupling the path's geometry from the design of the restoring fields, allowing generalizability to new paths. For bimanual tasks, it also enables the correct constrained motions without requiring local coordinates in the constraint set, requiring the object to be convex, or utilizing large forces to emulate object rigidity. Specifically, our contributions are:

1) A novel admittance control methodology for constrained pHRI, which is independent of the constraint geometry, does not require local coordinates within the constraint set, and is adjustable via a constraint strength parameter;

2) Theoretical proof of stability of the approach, demonstrating how motions within the constraint set are unaffected, and how the set is attractive and invariant;

3) Experimental verification of two motion constraints common in robot-assisted rehabilitation on two markedly different systems: (A) a path-guided reaching task with adjustable restoring force field, on the V-Rex full-body haptic exoskeleton, and (B) a bimanual virtual object interaction found in VR-based asymmetric bimanual rehabilitation, on the EXO-UL8 exoskeleton.

Demonstrating the applicability of the proposed unifying method on two prevalent robot-assisted rehabilitation tasks, on contrasting exoskeleton systems - existing on opposite ends of the task/joint space control, non-redundant/redundant, off-the-shelf (industrial)/custom, non-anthropomorphic/anthropomorphic spectra - further illustrates our method's generalizability and versatility.

II. METHODOLOGY

Our proposed approach requires an admittance control system, whose virtual dynamics represent the desired unconstrained pHRI motion. The constraint is then modeled as the zero level set of a smooth function that only depends on the virtual position. We introduce a parameter $\gamma \in [0,1] \subset \mathbb{R}$, called the *constraint strength*, which parameterizes how stringently the constraint is enforced; a value of $(\gamma = 0)$ corresponds to unconstrained motion, whereas $(\gamma = 1)$ fully constrains the motion. The max value represents a perfectly stiff constraint, which is necessary for emulating stable interaction with non-deformable virtual objects. Any intermediate value of γ allows for some violation of the constraint set that is also resisted by some restoring force, representative of typical behavior in path-guided rehabilitation schemes. Thus, desired behaviors in different robot-assisted rehabilitation applications can be achieved by γ, as summarized below:

$$\gamma \in \begin{cases} \{0\}, & \text{Unconstrained (nominal)}, \\ (0,1), & \text{Partially constrained}, \\ \{1\}, & \text{Fully constrained}. \end{cases} \quad (1)$$

A. Nominal Virtual Dynamics

Admittance control is commonly used for pHRI, in which human-applied forces are either measured or estimated, and then used to propagate virtual dynamics, which are typically second-order mass-damper systems [35]–[38]. These virtual systems' trajectories then become reference signals for the robot, which, assuming its controller is sufficiently performant, appears to move akin to the virtual dynamics. By assuming satisfactory tracking performance, only the virtual dynamics are considered from this point onward. Let $\theta(t) \in \mathbb{R}^n$ represent the generalized virtual position and $\tau(t) \in \mathbb{R}^n$ be the human-applied force, where n is the number of *degrees-of-freedom* (DoFs). For each DoF, the dynamics can be parameterized by virtual mass $m_i \in \mathbb{R}_{>0}$ and damping $b_i \in \mathbb{R}_{\geq 0}$:

$$m_i \ddot{\theta}_i(t) + b_i \dot{\theta}_i(t) = u_i(t), \quad (2)$$

where $i \in \{1, \ldots, n\}$, $u \in \mathbb{R}^n$ is the input to the virtual system, and $u(t) = \tau(t)$. The explicit dependency on time notation will be dropped for conciseness. The virtual second-order dynamics can include more complexity by treating each virtual link as a rigid body, resulting in the dynamics:

$$M(\theta)\ddot{\theta} + C(\theta, \dot{\theta}) + G(\theta) = u, \quad (3)$$

where $M(\theta) \in \mathbb{R}^{n \times n}$ is a positive-definite inertia matrix, $C(\theta, \dot{\theta}) \in \mathbb{R}^n$ represents the Coriolis and centripetal terms, and $G(\theta) \in \mathbb{R}^n$ is the gravity vector. Note that equation (2) can be written in the form of equation (3) by letting $M(\theta) = \text{diag}(m_1, \ldots, m_n)$, $C(\theta, \dot{\theta}) = \text{col}(b_1\dot{\theta}_1, \ldots, b_n\dot{\theta}_n)$, and $G(\theta) = 0_{n \times 1}$, where diag constructs a diagonal matrix from its arguments and col stacks its arguments. Define $x := (\theta, \dot{\theta}) \in \mathbb{R}^{2n}$ to be the state, which assumes a sufficiently large coordinate chart, and rewrite the dynamics as:

$$\dot{x} = \begin{bmatrix} \dot{\theta} \\ -M(\theta)^{-1}[C(\theta, \dot{\theta}) + G(\theta)] \end{bmatrix} + \begin{bmatrix} 0_{n \times n} \\ -M(\theta)^{-1} \end{bmatrix} u,$$
$$:= f(x) + g(x)u, \quad (4)$$

and define $f : \mathbb{R}^{2n} \to \mathbb{R}^{2n}$ and $g : \mathbb{R}^{2n} \to \mathbb{R}^{2n \times n}$ accordingly. Equation (4) is the general form of the nominal virtual dynamics, which will be used for subsequent sections.

B. Constraint Set Definition

To represent the constraint, let $h : \mathbb{R}^{2n} \to \mathbb{R}^k$ be at least a twice continuously differentiable function in the state, henceforth referred to as the constraint function, and satisfying $1 \leq k \leq n$ and $0_{k \times 1}$ being a regular value. Since only holonomic constraints are considered, let the constraints be modeled as equality constraints on the state using $h(x) = h(x_{1:n}) = 0_{k \times 1}$, where the $1 : n$ subscript refers to the first n coordinates of x. Next, define the constraint set to be the submanifold formed by the zero level set of h:

$$\Omega := \{x \in \mathbb{R}^{2n} \mid h(x) = 0_{k \times 1}\}. \quad (5)$$

Then, as long as the state can be restricted to Ω, the constraint equation is satisfied.

C. Objective Formulation

To formalize the constrained motion requirements, a time-invariant feedback control law $u(x, \gamma)$ should be designed to satisfy the following three objectives:

Objective 1 (Nominal): The dynamics should be unconstrained ($u = \tau$) and the same as the nominal dynamics for trajectories inside the constraint set. Moreover, when $\gamma = 0$, this requirement should hold over the entire domain $\mathbb{R}^{2n}$.

Objective 2 (Attractiveness): Unforced trajectories ($\tau = 0$) with initial conditions outside the constraint set should move towards it; i.e., $\inf_{x' \in \Omega} \|x(t) - x'\| \to 0$ as $t \to \infty$ for any $\gamma > 0$. However, when $\gamma = 1$, even forced trajectories ($\tau \neq 0$) should be attracted.

Objective 3 (Invariance): When the dynamics are fully constrained ($\gamma = 1$), any trajectory that enters the constraint set should remain there regardless of human-applied forces, τ; i.e., if $x(0) \in \Omega$, then $x(t) \in \Omega$ for all $t \geq 0$.

D. Virtual Constraints Controller

This subsection utilizes feedback linearization in order to decouple the virtual dynamics into components that are tangential and transversal to the constraint set. A stabilizing control law is then implemented on the transversal component, while human-applied forces are projected onto the tangential component. Define a virtual output $y = h(x)$ so that stabilizing Ω becomes output regulation of y. Then, the dynamics of y can be determined by differentiating it with respect to time:

$$y = h(x), \tag{6}$$

$$\dot{y} = \frac{\partial h}{\partial x} \dot{x} = \begin{bmatrix} \frac{\partial h}{\partial \theta} & 0_{k \times n} \end{bmatrix} \dot{x} = \mathcal{L}_f h(x), \tag{7}$$

$$\ddot{y} = \mathcal{L}_f^2 h(x) + \mathcal{L}_g \mathcal{L}_f h(x) u, \tag{8}$$

where $\mathcal{L}_f$ and $\mathcal{L}_g$ are the Lie operators along vector fields f and g, respectively. The dynamics of y are due to a vector relative degree of $(2, \ldots, 2)$ from the constraints being holonomic and the virtual dynamics of equation (4) being second-order, allowing the system with virtual output y to be input-output feedback linearizable [32]–[34], [39]. It is also assumed that the choice of h results in $\mathcal{L}_g \mathcal{L}_f h(x) \in \mathbb{R}^{k \times n}$ having linearly independent rows on $\Omega^c = \mathbb{R}^{2n} \setminus \Omega$, where the set is assumed to be nonempty. Then, for each $i \in \{1, \ldots, k\}$, define the coordinate transformation:

$$\eta^i(x) := \begin{bmatrix} h_i(x) \\ \mathcal{L}_f h_i(x) \end{bmatrix}, \tag{9}$$

so that its dynamics are linear for some virtual control input, $v_i = \mathcal{L}_f^2 h_i(x) + \mathcal{L}_g \mathcal{L}_f h_i(x) u$:

$$\dot{\eta}^i = \begin{bmatrix} 0 & 1 \\ 0 & 0 \end{bmatrix} \eta^i + \begin{bmatrix} 0 \\ 1 \end{bmatrix} v_i. \tag{10}$$

Each linear system η_i represents the dynamics of a component of y, so y can be regulated by stabilizing each η_i subsystem with a suitable state feedback:

$$v_i = -k_i \eta^i, \tag{11}$$

for some $k_i \succ 0_{1 \times 2}$, where $\succ$ refers to element-wise inequality. Although a linear controller suffices, any controller

$v_i(\eta_i)$ that stabilizes the origin of equation (10) stabilizes Ω. Note that $\eta := \mathrm{col}(\eta^1, \ldots, \eta^k) : \mathbb{R}^{2n} \to \mathbb{R}^{2k}$ is not a diffeomorphism unless $k = n$. When $k \neq n$, motion is allowed on the $n - k$ dimensional space Ω. By design, Ω consists of only the zero-dynamics, so the virtual constraint controller cannot interfere and the only forces that can act are human-applied forces. To determine the input u to the admittance controller, the virtual input $v := \mathrm{col}(v_1, \ldots, v_k)$ that stabilizes Ω needs to be transformed back into x-coordinates.

When $\gamma = 1$, the human-applied forces τ should not interfere with the stability of Ω, so its component in the subspace spanned by the rows of $\mathcal{L}_g \mathcal{L}_f h$ needs to be replaced by $v := \mathrm{col}(v_i, \ldots, v_k)$. The remaining component of τ respects the constraint and can be computed by projecting τ into the space tangential to the constraint manifold, which is the nullspace of $\mathcal{L}_g \mathcal{L}_f h$. Then, by using the Moore-Penrose inverse of $\mathcal{L}_g \mathcal{L}_f h$, the control input is:

$$\begin{aligned} u = {} & \tau - \gamma (\mathcal{L}_g \mathcal{L}_f h)^\dagger (\mathcal{L}_g \mathcal{L}_f h) \tau \\ & + \mathrm{sgn}(\gamma)(\mathcal{L}_g \mathcal{L}_f h)^\dagger (v - \mathcal{L}_f^2 h), \end{aligned} \tag{12}$$

where sgn is the signum function defined as:

$$\mathrm{sgn}(x) := \begin{cases} -1, & \text{if } x \leq 0, \\ 0, & \text{if } x = 0, \\ 1, & \text{if } x \geq 0. \end{cases} \tag{13}$$

The control law consists of three components:
1) τ, the nominal human-applied forces.
2) $-\gamma (\mathcal{L}_g \mathcal{L}_f h)^\dagger (\mathcal{L}_g \mathcal{L}_f h) \tau$, the γ-scaled component of τ in the space transversal to Ω. This term adjusts how much of the human-applied forces in the transversal direction are removed.
3) $\mathrm{sgn}(\gamma)(\mathcal{L}_g \mathcal{L}_f h)^\dagger (v - \mathcal{L}_f^2 h)$, the virtual transversal stabilizing controller transformed back to x-coordinates.

The proposed control law leads to the following result.

Theorem 1. *The control law of equation (12) satisfies the three main objectives: (1) nominal, (2) attractiveness, and (3) invariance.*

Proof of Theorem 1. To satisfy the first objective, consider a trajectory $x(t) \in \Omega$. Then, since $h(x)$ is identically zero for this trajectory, the matrix $\mathcal{L}_g \mathcal{L}_f h(x)$ and its Moore-Penrose pseudoinverse are also zero, of dimension $k \times n$ and $n \times k$, respectively. Thus, substituting these matrices into the control law of equation (12) reduces it to $u = \tau$, which is independent of γ, as required. Furthermore, when $\gamma = 0$, the control law also reduces to $u = \tau$. These two cases together satisfy **Objective 1**.

To show that the last two objectives can by satisfied by the control law of equation (12), consider the error dynamics away from Ω. Let the error $e \in \mathbb{R}^n$ be defined as $e := h(x)$, so that its closed-loop dynamics are:

$$\dot{e} = \mathcal{L}_f h, \tag{14}$$

$$\begin{aligned} \ddot{e} = {} & \mathcal{L}_f^2 h + (\mathcal{L}_g \mathcal{L}_f h) \tau \\ & - \gamma (\mathcal{L}_g \mathcal{L}_f h)(\mathcal{L}_g \mathcal{L}_f h)^\dagger (\mathcal{L}_g \mathcal{L}_f h) \tau \\ & + \mathrm{sgn}(\gamma)(\mathcal{L}_g \mathcal{L}_f h)(\mathcal{L}_g \mathcal{L}_f h)^\dagger (v - \mathcal{L}_f^2 h), \end{aligned} \tag{15}$$
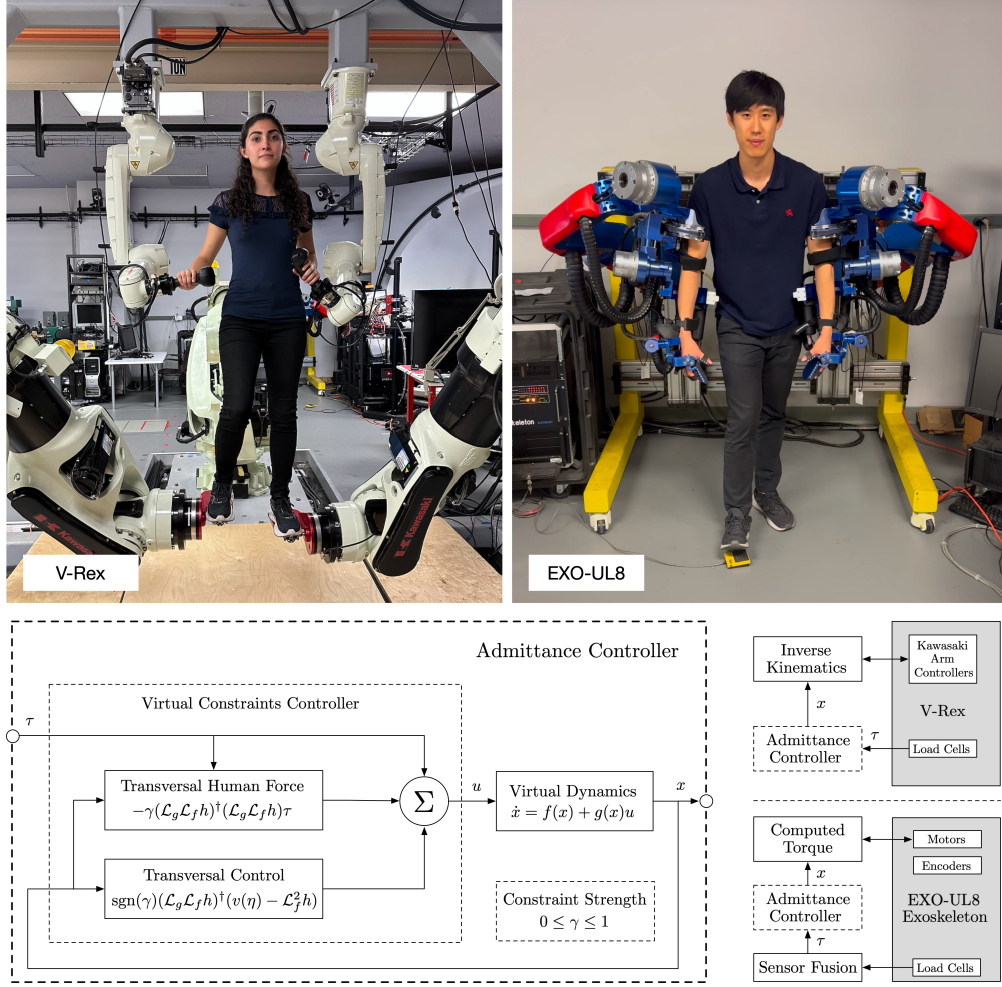
Fig. 1. (Top left) The V-Rex is a full-body haptic system consisting of five robotic serial manipulators interacting with the operator in task-space through the hands, feet, and a harness at the pelvis. (Top right) The EXO-UL8 is a bimanual upper-limb exoskeleton interacting with the operator in joint-space through three force/torque sensors per arm. (Bottom) The admittance controller consists of the virtual constraints controller of equation (12) and the virtual dynamics of equation (4). The virtual constraints controller replaces the γ-scaled component of the nominal human-applied force in the transversal direction with the output of a transversal stabilizing controller. The value of γ determines how strongly the operator can push back against the constraint. The same admittance controller structure can be used in both the V-Rex and EXO-UL8 exoskeletons, even though they have different virtual dynamics and constraint functions.

which substitutes equation (12) into the virtual dynamics of equation (4). By the assumption that $\mathcal{L}_g \mathcal{L}_f h$ has linearly independent rows, and is rank k, $(\mathcal{L}_g \mathcal{L}_f h)(\mathcal{L}_g \mathcal{L}_f h)^\dagger = I_{k \times k}$. Thus, equation (15) reduces to:

$$\ddot{e} = \mathcal{L}_f^2 h + (1-\gamma)(\mathcal{L}_g \mathcal{L}_f h)\tau + \text{sgn}(\gamma)(v - \mathcal{L}_f^2 h). \quad (16)$$

Considering the last two objectives, there are two cases of interest: (1) $\gamma > 0$ with unforced dynamics ($\tau = 0$), and (2) $\gamma = 1$ and any value of τ. These cases correspond to partially and fully constraining the dynamics to Ω, respectively. However, in either case, equation (16) simplifies to:

$$\ddot{e} = v. \quad (17)$$

By defining $\epsilon := \text{col}(e_1, \dot{e}_1, \ldots, e_k, \dot{e}_k)$, the error dynamics become:

$$\dot{\epsilon} = \left(I_{k \times k} \otimes \begin{bmatrix} 0 & 1 \\ 0 & 0 \end{bmatrix} \right) \epsilon + \left(I_{k \times k} \otimes \begin{bmatrix} 0 \\ 1 \end{bmatrix} \right) v, \quad (18)$$

where $\otimes$ is the Kronecker product. Then, substitute in the virtual control law of equation (11) by observing that $\epsilon = \eta$.

The closed-loop error dynamics of equation (18) then becomes block-diagonal:

$$\dot{\epsilon} = \text{diag}\left(\begin{bmatrix} 0 & 1 \\ -k_{1,1} & -k_{1,2} \end{bmatrix}, \ldots, \begin{bmatrix} 0 & 1 \\ -k_{k,1} & -k_{k,2} \end{bmatrix} \right) \epsilon, \quad (19)$$

where the matrix is formed as the block diagonal of all the 2×2 blocks. Its eigenvalues are the union of the eigenvalues of each 2×2 block. By the Routh-Hurwitz criteria, each block's eigenvalues are in the open left half-plane if $k_i \succ 0_{1 \times 2}$ for all $i \in \{1, \ldots, k\}$. Thus, the error dynamics can be stabilized by an appropriate choice of gains k_i. It is worth noting that although the η-dynamics are linear, the choice of a virtual transversal controller v does not have to be linear. The feedback linearization allows the system dynamics of equation (4) to be decoupled into transversal and tangential subsystems, so the choice of a stabilizing transversal controller is flexible. In any case, the stability of ϵ holds everywhere in the domain, which satisfies **Objective 2** and **Objective 3**. ■

The implementation of the virtual constraints controller within the admittance controller is shown in Fig. 1.

4

III. Experimental Setup

In order to demonstrate the versatility of the proposed method, two experiments are conducted on different exoskeletons: a path-based reaching task with restoring force field, and bimanual manipulation of a virtual rigid object. The first experiment demonstrates how the proposed methodology can emulate the restoring force fields commonly found in path-based schemes [7]–[17]. The second experiment shows how the methodology ensures stable interaction with rigid virtual objects, a prevalent challenge in VR-based pHRI applications [2], [3], [6], [24], [27]. Whereas the first experiment varies the constraint strength parameter in order to replicate varying restoring force field strengths, the second experiment maximizes the parameter to emulate a perfectly rigid virtual object. The second experiment is also in a much higher dimensional space, showing the methodology's advantage of not requiring local coordinates. Together, these two distinct experiments highlight the broad applicability of constrained admittance control enabled by the proposed methodology. A depiction of the experiments is shown in Fig. 2. For each experiment, the pertinent exoskeleton system is first introduced, and then the constraint modeling associated with the task is described.

A. Path-Based Reaching Task

1) V-Rex Full-Body Haptic Exoskeleton: The Virtual Reality Exoskeleton (V-Rex) is a non-anthropomorphic full-body haptic system consisting of five Kawasaki industrial serial manipulators. Two RS-007L manipulators interact with the operator's hands, two BX-100S manipulators are connected with safety breakaways at the feet, and one CX-210L provides gravity offloading through a harness attached at the pelvis. Each of the five manipulators has six powered revolute DoFs, is independently controlled in task-space, and is also equipped with a six-DoF force/torque sensor at the end effector. Nominal motion via admittance control with the upper-left manipulator is accomplished by integrating the force measurement at the end effector to propagate a virtual second-order model of the form in equation (2) in 3D. The virtual model parameters used are mass: 10 kg and damping: 15 Ns/m, which were selected empirically to enable agile motions while remaining stable. The virtual trajectory is then transformed into joint-space using an inverse kinematics solver, before serving as reference signals for the embedded Kawasaki arm controller. Fig. 1 shows the V-Rex and a block diagram of its control.

2) Elliptical Path Constraint with Restoring Force Field: A path constraint can be implemented with varying levels of constraint strength, ranging from free motion ($\gamma = 0$) to fully constrained ($\gamma = 1$). To illustrate how γ affects the interaction forces and corresponding trajectories during path-based reaching tasks, a constraint set Ω is implemented in the form of an ellipse, while a different ellipse oriented $90°$ from the first is used as a target trajectory. Both ellipses are situated in the $x_3 = 0$ plane (parallel to the ground). The operator attempts to move along the target trajectory, even though the virtual constraints controller is pushing them onto Ω. Although the interaction is through the hand, the setup serves to demonstrate the methodology and can be modified
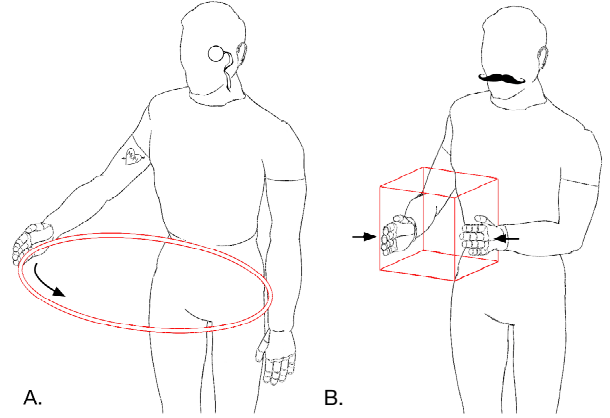

Fig. 2. The two robot rehabilitation tasks in this study are: (A) a unilateral reaching task constrained to an elliptical path by an adjustable restoring force field, typically found in path-guided rehabilitation, and (B) a bimanual manipulation task of a virtual rigid object, commonly found in VR-based robot rehabilitation. For each task, the submanifold of allowable motions is modeled as a smooth function's level set, and then used by the virtual constraints controller to restrict nominal motions to the submanifold. The tasks are experimentally verified on the V-Rex full-body haptic exoskeleton and the EXO-UL8 upper-limb bimanual exoskeleton, respectively.

to simulate human gait. Equation (20) shows the elliptical path constraint, with x_{1c} and x_{2c} defined as the ellipse center, and the minor and major axes $a = 0.15$m and $b = 0.2$m chosen to fit within the V-Rex's workspace:

$$h(x) = \begin{bmatrix} h_1(x) \\ h_2(x) \end{bmatrix} = \begin{bmatrix} \frac{(x_1 - x_{1c})^2}{a^2} + \frac{(x_2 - x_{2c})^2}{b^2} - 1 \\ x_3 \end{bmatrix}. \quad (20)$$

The target ellipse has parameters $a = 0.2$m and $b = 0.15$m and is drawn on a table below the manipulator, serving as a visual aid for the operator, as show in Fig. 3. Constraint strengths of $\gamma \in \{0.0, 0.3, 0.7, 1.0\}$ are used for the trials. The path constraint is enforced through a force field generated by a virtual spring damper system, similar to [16]. This choice of force field does not limit the system as any other stabilizing field can be used, depending on the desired performance. Furthermore, the experiment aims to demonstrate the main advantage that the transversal component of the constraint is isolated, allowing the stabilizing force fields to be developed independently of the path's geometry.

B. Bimanual Interaction with Virtual Object

1) EXO-UL8 Bimanual Upper-Limb Exoskeleton: The EXO-UL8 is a custom bimanual powered redundant upper-limb anthropomorphic exoskeleton consisting of two arms, each with seven revolute DoFs [21], [22], [35], [40]. Each arm is equipped with three six-DoF force/torque sensors located at the upper arm, lower arm, and wrist. The measured force/torque signals are first fused using the method from [22], before propagating the virtual dynamics of the admittance control in joint space, which is 14-dimensional and consists of 14 independent second-order systems of the form of equation (2). The motions of this virtual system determine the nominal motion of the exoskeleton. The combined virtual state then serves as a reference signal that a computed torque controller [41] tracks. The virtual system parameters were selected empirically to be agile while remaining stable, and are shown in Tab. I. Fig. 1 shows the system and its control architecture.
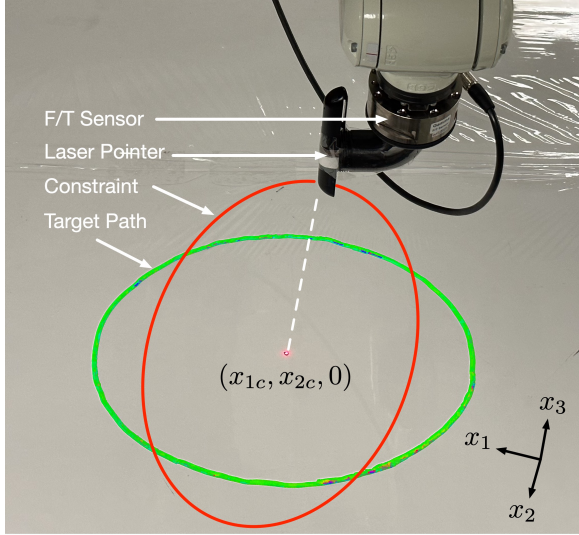
Fig. 3. The path experiment uses the upper-left arm of the V-Rex constrained to an ellipse (red) with varying constraint strengths, parameterized by γ. The operator attempts to follow the target path (green), which is also an ellipse but rotated $90°$ about the x_3-axis in order to illustrate the effect of γ. A laser pointer mounted at the end effector helps to visualize the 2D projection of the motion onto the plane containing the two ellipses.
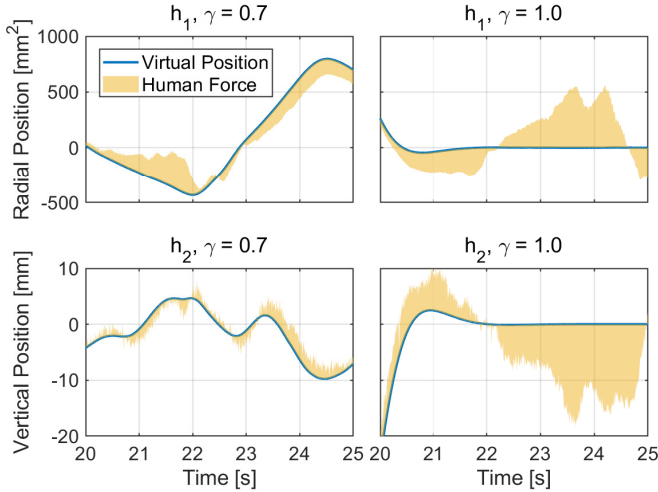

Fig. 4. The transversal states of the path-constrained reaching experiment as defined in equation (20) and corresponding human-applied forces are shown as timeseries for constraint strengths: $\gamma = 0.7$ (left), and $\gamma = 1.0$ (right). Human-applied forces and the virtual constraints controller's output influence the virtual position when $\gamma = 0.7$, allowing the operator to deviate from the constraint while experiencing a restoring force. However, when $\gamma = 1.0$, the virtual position stabilizes independently of any human-applied force.

2) Relative Pose Constraint: Bimanual interaction with virtual rigid objects involves constraining the 14-dimensional space of motions to the subset in which the relative pose between the end effectors is constant. To formulate this constraint, let $T_l, T_r \in \mathrm{SE}(3)$ be the homogeneous transformation from the base (inertial) frame to the left and right end effectors, respectively. Using the *product-of-exponentials* formulation, each transformation can be written as a map of the joint angles:

$$T_l(\theta^l) = \left(\prod_{i=1}^{7} e^{\hat{\xi}_i^l \theta_i^l} \right) T_l(0), \tag{21}$$

Left/Right Joint	Inertia ($\mathrm{kg \cdot m^2}$)	Damping ($\mathrm{kg \cdot m^2/s}$)
1	0.5	2.5
2	0.5	2.0
3	0.25	1.0
4	0.25	1.0
5	0.125	1.0
6	0.05	2.0
7	0.05	2.0

where $\{\xi_i^l\}_{i=1}^{7}$ are the twists in local coordinates associated with each of the left joints, and $T_l(0)$ is the transformation in the default configuration. Similarly for the right arm, T_r is a function of θ^r, and parameterized by the right twists $\{\xi_i^r\}_{i=1}^{7}$. Then, the relative transformation between the end effectors is $T_{rl}(\theta^r, \theta^l) = T_r^{-1}(\theta^r) T_l(\theta^l)$. Using local coordinates for $\mathrm{SE}(3)$, and defining $\theta := (\theta^r, \theta^l)$, the constraint function is:

$$h(\theta, \dot{\theta}) = [p(\theta), \alpha(\theta)] - (p_0, \alpha_0), \tag{22}$$

where $(p(\cdot), \alpha(\cdot)) : \mathbb{R}^{14} \to \mathbb{R}^3 \times \mathbb{R}^3$ are local coordinates for $T_{rl}(\theta)$, and $(p_0, \alpha_0) \in \mathbb{R}^3 \times \mathbb{R}^3$ is the desired constant relative pose between the end effectors. The coordinates of the desired relative pose, (p_0, α_0), are measured when contact is first made with the virtual object. Note that the choice of local coordinates on $\mathrm{SE}(3)$ does not matter as long as they exist over the range of the desired motion. In our experiments, canonical coordinates are used for position and ZYX Tait-Bryan angles for orientation. Specifically, given matrix coordinates for a relative pose, $T_{rl} \in \mathrm{SE}(3)$:

$$T_{rl}(\theta) = \begin{bmatrix} R(\theta) & p(\theta) \\ 0 & 1 \end{bmatrix}, \tag{23}$$

$$\alpha(\theta) = \begin{bmatrix} \sin^{-1}(-R_{21}(\theta)/\sqrt{1 - R_{31}(\theta)^2}) \\ \sin^{-1}(-R_{31}(\theta)) \\ \sin^{-1}(-R_{32}(\theta)/\sqrt{1 - R_{31}(\theta)^2}) \end{bmatrix}, \tag{24}$$

where the coordinate chart is defined on the subset of $\mathrm{SE}(3)$ in which $R_{31} \neq \pm 1$. A high-dimensional motion set with a constraint manifold $\Omega = h^{-1}(0)$ for which local coordinates on Ω are hard to find demonstrates the generalizability of the proposed feedback linearization-based approach.

C. Derivation of Transversal Forces

To allow visualization, the transversal components of the human-applied forces can be extracted by projecting the sensor-measured human-applied forces, $\tau \in \mathbb{R}^n$, into the transversal directions, which are obtained from the first n columns of each row of the Jacobian of the constraint function ($h : \mathbb{R}^{2n} \to \mathbb{R}^k$) and then unit-normalized. Since the constraint set is a submanifold, the Jacobian of the constraint function is non-singular when evaluated on the constraint set, which is where the visualization is plotted. The human-applied forces can then be projected using these unit vectors to get its transversal component. Let $N(x) = \begin{bmatrix} \cdots & \hat{n}_i(x)^\top & \cdots \end{bmatrix}^\top \in$
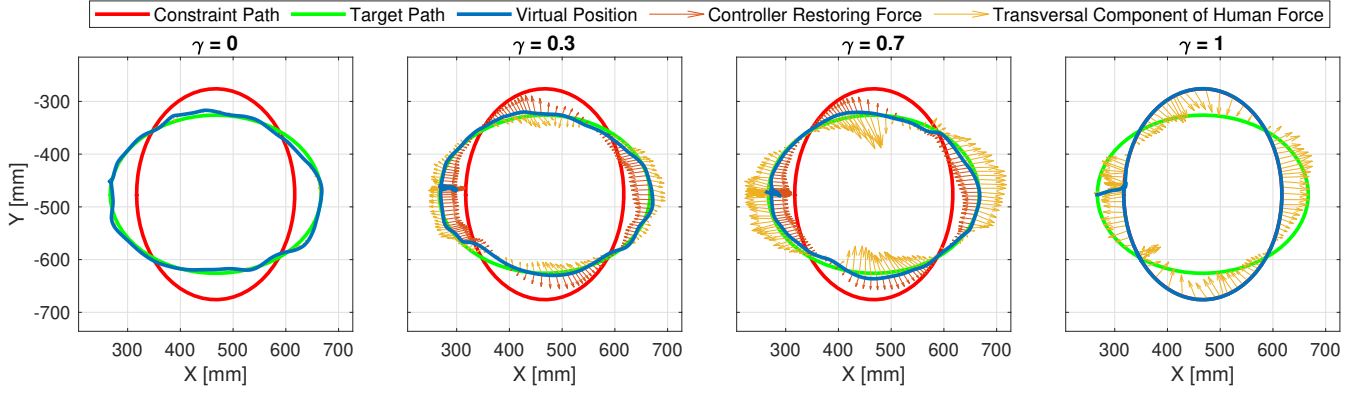
Fig. 5. The manipulator's trajectory (blue line), the controller's restoring force, and the transversal component of the human-applied force (scaled for better visualization) are plotted for each trial. The operator attempts to follow a target trajectory oriented $90°$ (green line) from the constraint set (red line). In the unconstrained trial ($\gamma = 0$), no restoring forces are present and the operator can follow the target, as expected. When the motion is partially constrained ($0 < \gamma < 1$), the virtual constraints controller generates restoring forces transversal to the constraint (red arrows), which push the motion towards the constraint set. The transversal components of the human-applied forces (yellow arrows) are plotted to show how the operator has to apply more force in the $\gamma = 0.7$ trial than in the $\gamma = 0.3$ trial since γ scales how much of the human forces is present in the transversal direction. Note that the controller's restoring forces are independent of $\gamma > 0$ as designed in equation (12). When fully constrained ($\gamma = 1$), no amount of human force is able to move the position away from the constraint as shown by the trajectory aligning perfectly with the constraint path. Each trial took approximately 30 seconds to complete.

$\mathbb{R}^{k \times n}$, where $\hat{n}_i(x) \in \mathbb{R}^{1 \times n}$ is the unit-normalized vector of $n_i(x)$, which is defined as:

$$n_i(x) := \hat{e}_i^\top \frac{\partial h}{\partial x}(x) \begin{bmatrix} I_{n \times n} \\ 0_{n \times n} \end{bmatrix}, \tag{25}$$

and $\hat{e}_i$ is the ith unit basis vector. Then, the transversal component of τ can be computed as $N(x)\tau$.

D. Software Implementation and Numerical Considerations

While computing the gradient and Hessians for h in the elliptical path constraint of equation (20) may be tractable, the same quantities for the relative pose constraint of equation (22) require significantly more work. To ensure correctness and minimize the impact of numerical errors, symbolic tools, such as SymForce [42] or Sympy [43], can symbolically differentiate the quantities and generate corresponding optimized C++ code that can be evaluated quickly online.

Note that when $x \in \Omega$, $h(x) = 0$, so the matrix $\mathcal{L}_g \mathcal{L}_f h(x)$ and its Moore-Penrose inverse are also zero, of dimension $k \times n$ and $n \times k$, respectively. In practice, when floating-point arithmetic is used, care should be taken to ensure that numerically small values in $\mathcal{L}_g \mathcal{L}_f h(x)$ are treated as zero. Specifically, each row of $\mathcal{L}_g \mathcal{L}_f h(x)$ should first be checked for whether it is numerically non-zero; call the set of non-zero row indices $NZ(x) \subseteq \{1, \ldots, k\}$. Next, form the matrix $L = \text{row}(r_1, \ldots, r_k)$, where row r_i is defined as:

$$r_i := \begin{cases} \text{row } i \text{ of } \mathcal{L}_g \mathcal{L}_f h(x), & \text{if } i \in NZ(x), \\ 0_{1 \times n}, & \text{otherwise.} \end{cases} \tag{26}$$

Then, any instance of the vector $(\mathcal{L}_g \mathcal{L}_f h(x))^\dagger w$, where $w \in \mathbb{R}^k$, as in the case of equation (12), can be written as a linear combination of non-zero columns of $L^\dagger$:

$$(\mathcal{L}_g \mathcal{L}_f h(x))^\dagger w \approx \sum_{i \in NZ(x)} (L^\dagger)_i w_i, \tag{27}$$

where $(L^\dagger)_i$ is the ith column of $L^\dagger$.

IV. RESULTS

A. Path-Based Reaching Task

The path-based reaching task assesses the controller with four constraint strengths, ranging from free motion ($\gamma = 0$) to fully constrained ($\gamma = 1$). The operator starts at the left-most edge of the target ellipse (-200mm, -450mm) and the virtual constraints controller is activated. Fig. 4 shows the transversal states of equation (20) as a function of time. When $\gamma = 1$, the states converge to zero regardless of the human-applied forces, as expected. When $0 < \gamma < 1$, the human-applied forces can resist the controller and prevent the state from reaching zero, as shown in the left column of Fig. 4 and the middle subfigures of Fig. 5. In these cases, the operator haptically experiences the restoring force field generated by the controller.

Fig. 5 plots the motion trajectories, with the transversal component of the human-applied forces and the virtual constraint controller's output overlaid. During free motion ($\gamma = 0$), there are no constraint-enforcing forces. In the partially constrained cases ($\gamma = 0.3, \gamma = 0.7$), the operator can guide the robot along the target path; however, the motion is partially resisted, resulting in transversal forces pushing towards the constraint. This controller output is not affected by γ as shown in equation (12), and is only a function of the system's state, resulting in minimal variation in the two partially constrained trials. On the other hand, equation (12) shows that as γ increases, a larger proportion of the transversal component of the human-applied forces is removed. As a result, the operator must exert more force to maintain the target trajectory, which is shown by the larger human-applied force arrows in the $\gamma = 0.3$ and $\gamma = 0.7$ cases of Fig. 5. In the fully constrained case ($\gamma = 1$), the robot's trajectory remains on the constraint path despite the human-applied forces pushing towards the target path.

B. Bimanual Interaction with Virtual Object

The bimanual interaction starts with the operator in the EXO-UL8 freely moving each arm, shown in subfigure 1 of
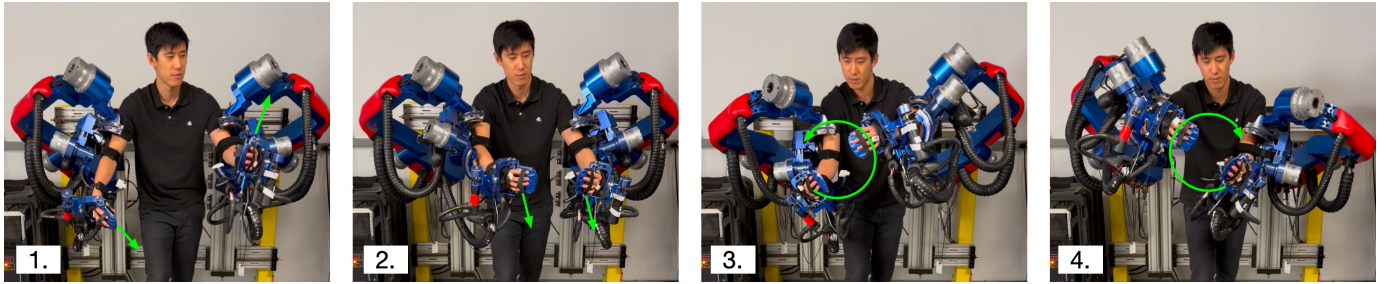
Fig. 6. Subimages show keyframes of the bimanual interaction with a virtual object. The object is not explicitly defined by its geometry, but rather as a constraint on the total joint space in which the relative pose between the hands is fixed. During keyframe (1), the hands are unconstrained ($\gamma = 0$). In keyframe (2), the constraint is activated by setting $\gamma = 1$. Subsequent motions (2)-(4) show that the virtual rigid coupling between the hands gives the illusion of interacting with a virtual rigid object that can be freely manipulated.
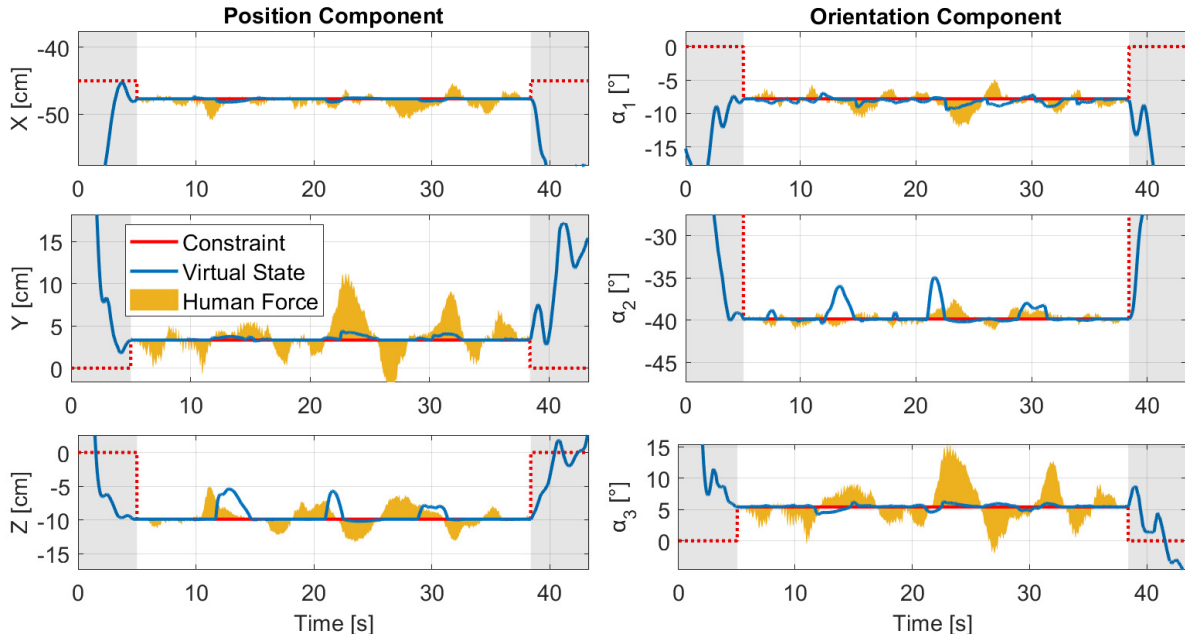

Fig. 7. Subplots show the six local coordinates of the transversal state of the relative pose between the EXO-UL8's end effectors as defined in equation (22), where X, Y, Z correspond to position, and $\alpha_1, \alpha_2, \alpha_3$ correspond to orientation. The gray regions show unconstrained motion ($\gamma = 0$), during which the constraint values are not set (dashed red lines), whereas the region in the middle is fully constrained ($\gamma = 1$). Since the desired pose is snapshot at the start of the constrained motion (left edge of gray region), the virtual state (blue) is equal to the constraint value (red) at this point in time. During the constrained motion, the virtual constraints controller tracks the constraint while rejecting any human-applied forces in the transversal direction (orange) that push the virtual state away from the constraint manifold. Note that the spikes in the virtual state are explained in Fig. 8.

Fig. 6. Once the operator's hands are in a desired configuration, e.g., around a virtual object, the relative pose between the hands is measured as (p_0, α_0), which is used in the constraint function of equation (22). The virtual constraints controller is activated by setting the constraint strength to $\gamma = 1$, as shown at the left gray boundary in Fig. 7. Subsequent motion within the constraint set physically appears as the hands being rigidly coupled, as seen in subfigures $2 - 4$ of Fig. 6, emulating interaction with a virtual rigid object.

Furthermore, during this time the component of the human interaction force transversal to the constraint set does not impact the constraint controller's tracking performance as shown in Fig. 7, which is expected since $\gamma = 1$. The remaining tangential component of the interaction force component allows the virtual object (a relative pose between the end effectors) to move only in the $14 - 6$ dimensional joint space constraint manifold, as illustrated by subfigures $2 - 4$ of Fig. 6. Once the interaction is complete, the constraints are deactivated by setting $\gamma = 0$ at the right gray boundary in

Fig. 7, and the hands can move independently again.

V. DISCUSSION

A. Advantages Over Existing Approaches

The two experiments showcase the prominent features of our approach, namely its abilities to:

1) enable constrained pHRI independently of the constraint geometry (both experiments),
2) overcome the requirement of local coordinates for the constraint manifold (both experiments).
3) adjust the constraint strength in order to emulate commonly used force fields (first experiment),
4) enable stable interaction with stiff virtual objects without requiring convexity (second experiment).

In order to compare the advantages of our constrained admittance control approach to the state-of-the-art, the following relevant metrics are used: (1) generalizability, which specifies the classes of constraints supported due to parameterization

TABLE II
RELATIVE COMPARISON TO STATE-OF-THE-ART APPROACHES

Study\Metric	Generalizability	Switching	Computation
He [7]	Path, 2D Surface −	Gains −	Iterative −
Selvaggio [8]	Path −	Continuous gains =	Iterative (Newton's method) −
Shi [11]	Path −	Continuous torque profiles =	Iterative (Newton's method) −
Asl [14]	Path −	Continuous force profiles =	Sampling −
Ours	Zero level set of h	None	Analytical

Fig. 8. The instances (pale red) when the virtual Z-position (blue) deviates from the constraint set (around -10cm) in the bottom left subfigure of Fig. 7 is caused by joint 6 (wrist flexion/extension) of the EXO-UL8's right arm (green) reaching its lower mechanical limit (dashed black line). Since the joint cannot physically go lower, the virtual position cannot maintain its set point. A similar case is evident in the α_2-orientation component of the virtual state.

requirements; (2) switching, which indicates whether switching between different schemes or control gains is necessary depending on whether the constraint is active; and (3) computation, which gauges the approach's algorithmic complexity. Some studies, namely [7], [8], [11], [14], only handle path-based constraints because the allowable motion tangential to the path can be parameterized, such as by arc length. However, these approaches would not generalize well to higher dimensional manifolds for which finding a parameterization may be intractable. Thus, the first metric captures the limitation in this regard. The second metric is concerned about switching behavior of controller gains or restoring force profiles at the constraint boundary, which could adversely affect stability. For instance, [14] defines a tunnel around the path and has different, but continuous, force profiles depending on the robot's position, and [7] implements gain scheduling based on the robot's position relative to the constraint boundary. Lastly, many approaches require finding the point on the constraint set that is minimal distance to the robot's position in order to construct a direction in which a constraint-enforcing scheme could act [7], [8], [11]. However, the method for finding the point is often iterative and is an optimization problem in itself, which may detract from real-time performance. Thus, the computation metric indicates whether iterative subroutines are necessary. A comparison of our approach with existing approaches using these three metrics is given in Table. II. Each comparison is indicated by $-$ or $=$ to indicate less performant or comparable to ours, respectively.

1) Path-Based Reaching Task: This experiment utilized a virtual spring damper system to generate the corrective force field transversal to the constraint path in order to demonstrate how our approach can emulate existing experiments found in the literature. However, our method is advantageous in that the force field is completely agnostic of the constraint path's geometry, and can be generated by any stabilizing controller. Furthermore, while the experiment utilizes a closed elliptical path for demonstrating the path constraint, which is commonly found in path-guided rehabilitation tasks, our proposed method is not limited to a specific path or robotic system. Unlike many existing control schemes for path following that require either a parameterized path or one comprised of timed waypoints, our method is time-invariant and can be applied to any valid path
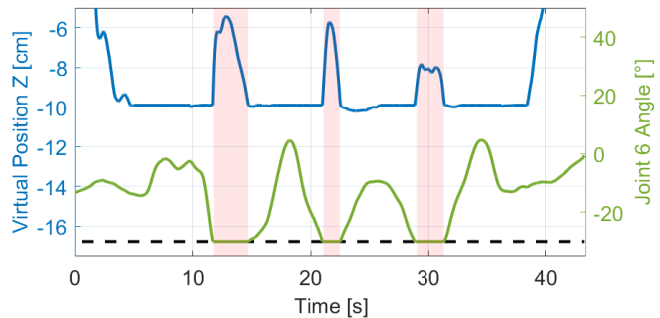
without requiring a parameterization for the submanifold, and any admittance control rehabilitation robot utilizing second-order virtual dynamics.

2) Bimanual Interaction with Virtual Object: The virtual constraints controller enables bimanual interaction with virtual rigid objects by constraining the relative pose between the operator's hands. This experiment highlights the distinction of our approach in that it does not require local coordinates for the constraint manifold. The space of allowable motions for this bimanual interaction constraint corresponds to a $14-6 = 8$ dimensional submanifold, for which finding a local parameterization is difficult. The approach is also agnostic to the geometry of the virtual object when constraining the motion, which places no restrictions on the shape of the object, such as convexity. The only place in which the object's geometry is used is in detecting initial contact in order to record (p_0, α_0). However, detecting contact is much simpler than constraining dynamics to respect their geometries, which is typically done in force-based approaches. The proposed method also does not suffer from instability of contacting high-stiffness objects, making it appropriate for virtual interactions in VR-based rehabilitation applications.

B. Effects of Physical Joint Limits

In the Z-position and α_2-orientation subplots of Fig. 7, the virtual state appears to deviate from the constraint manifold at 13s, 22s, and 30s. This behavior is not a limitation of the virtual constraints controller, but rather due to the hard joint limits of the EXO-UL8. At these instances, joint 6 of the right arm reaches its minimum allowed value of $-30°$ as shown in Fig. 8, so the corresponding virtual states h cannot maintain its set points of $h_3 = -10$ cm and $h_5 = -40°$.

C. Limitations and Possible Extensions

1) Nonholonomic Constraints: The use of second-order virtual dynamics in the admittance control is to make the physical interaction predictable by leveraging our intuition of how rigid bodies move. In the virtual constraints controller, this choice manifests as the transversal output having a vector relative degree of 2 due to the virtual constraints being holonomic.
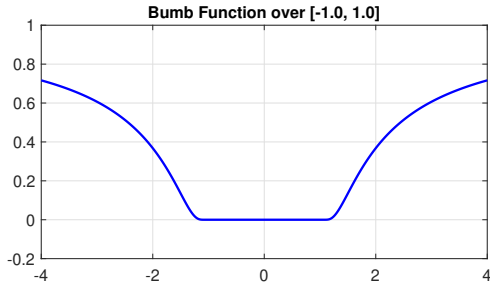
Fig. 9. A 1D bump function of the form of equation (28) over the interval $[-1, 1]$. Note that the function is smooth everywhere and only zero on the desired interval. The zero level set of the function forms the desired bounding region, normally specified with inequality constraints.

However, the method can extend to non-holonomic constraints with virtual dynamics of any order by following the same approach, as long as the virtual outputs remain input-output feedback linearizable.

2) Inequality Constraints: One limitation of the approach arises in modeling the constraint set as the zero level set of an equality constraint: $h(x) = 0$. The consequence of this is that modeling bounding regions (e.g., $a \leq x \leq b$ in 1D) or manifolds with boundaries is not possible. However, if $h(x)$ is not required to be analytic, then this can be done using bump functions, where a 1D case is shown below:

$$b(x) := \begin{cases} e^{\frac{1}{x-a}} & , \quad x < a, \\ 0 & , \quad a \leq x \leq b, \\ e^{-\frac{1}{x-b}} & , \quad b < x. \end{cases} \quad (28)$$

Fig. 9 shows $b(x)$. Note that $b(x)$ is smooth everywhere on its domain, and is only zero on the desired interval $[a, b]$. Thus, $h(x) = b(x)$ can be used as the desired constraint function. The zero level set of $h(x)$ is the desired constraint set, so trajectories are bounded within $[a, b]$.

3) Global Asymptotic Stability: The proposed methodology utilizes feedback linearization, which has inherent limitations in that results are local. In general, the state space could be a smooth manifold rather than $\mathbb{R}^{2n}$. The choice of local coordinates assumes that all trajectories of the dynamics are in the same sufficiently large coordinate chart. Consequently, the asymptotic stability results of Theorem 1 are only presented in this coordinate chart. However, a smooth manifold has smoothly compatible coordinate charts, so relevant coordinate transformations can extend the dynamics and the proposed controller. But, additional care must be taken to correctly apply transformations when switching between coordinate charts.

4) Point-to-Point Trajectories: Although gait rehabilitation consist of cyclic trajectories akin to the first experiment, many upper-limb rehabilitation tasks consist of reach-to-grasp motions in which the subject follows straight line segments to move in a point-to-point fashion. Frenet-Serret frames cannot be directly applied to define a constraint function due to the lack of curvature. However, if a convention for pointing either the normal/binormal direction is defined a priori, then the constraint function could be constructed as the distances along these directions. End points of the line segment can additionally be enforced via the aforementioned method on implementing inequality constraints.

VI. CONCLUSION

This study presents a novel feedback linearization-inspired method for constraining admittance control to virtual subsets, without explicit dependency on the constraint geometry. Two prevalent rehabilitation exoskeleton applications are explored: a path-guided reaching task, and a bimanual interaction with a virtual object. In the first experiment, the method constrains motion to an elliptical path using a virtual spring damper restoring force field. A constraint strength parameter limits how much the operator can resist the constraint, serving as an analogue for the restoring force field strength. In the second experiment, the method constrains end effectors of a bimanual exoskeleton in its 14-dimensional joint space to simulate stable interaction with a rigid virtual object, demonstrating its advantage in not requiring local coordinates to represent allowable motions. Experimental results illustrate the virtual constraint controller's stability against constraint-violating forces, while remaining transparent to permissible motions. The experiments highlight the methodology's versatility and generalizability for enabling constrained pHRI for rehabilitation exoskeletons.

REFERENCES

[1] Y. Shen, P. W. Ferguson, and J. Rosen, "Chapter 1 - upper limb exoskeleton systems—overview," in *Wearable Robotics* (J. Rosen and P. W. Ferguson, eds.), pp. 1–22, Academic Press, 2020.

[2] O. Mubin, F. S. Alnajjar, N. Jishtu, B. S. Alsinglawi, and A. A. Mahmud, "Exoskeletons with virtual reality, augmented reality, and gamification for stroke patients' rehabilitation: Systematic review," *JMIR Rehabilitation and Assistive Technologies*, vol. 6, 2019.

[3] W. Qi, S. Sun, T. Niu, and D. Zhao, "Research and prospects of virtual reality systems applying exoskeleton technology," *Universal Access in the Information Society*, pp. 1–22, 2022.

[4] Q. Ai, Z. Liu, W. Meng, Q. Liu, and S. Q. Xie, "Machine learning in robot assisted upper limb rehabilitation: A focused review," *IEEE Transactions on Cognitive and Developmental Systems*, pp. 1–1, 2021.

[5] U. P. Matic Trlep, Matjaž Mihelj and M. Munih, "Rehabilitation robot with patient-cooperative control for bimanual training of hemiparetic subjects," *Advanced Robotics*, vol. 25, no. 15, pp. 1949–1968, 2011.

[6] E. D'Antonio, E. Galofaro, F. Patané, M. Casadio, and L. Masia, "A dual arm haptic exoskeleton for dynamical coupled manipulation," in *2021 IEEE/ASME International Conference on Advanced Intelligent Mechatronics (AIM)*, pp. 1237–1242, 2021.

[7] Y. He, Y. Hu, P. Zhang, B. Zhao, X. Qi, and J. Zhang, "Human–robot cooperative control based on virtual fixture in robot-assisted endoscopic sinus surgery," *Applied Sciences*, vol. 9, no. 8, 2019.

[8] M. Selvaggio, G. A. Fontanelli, F. Ficuciello, L. Villani, and B. Siciliano, "Passive virtual fixtures adaptation in minimally invasive robotic surgery," *IEEE Robotics and Automation Letters*, vol. 3, no. 4, pp. 3129–3136, 2018.

[9] M. M. Marinho, H. Ishida, K. Harada, K. Deie, and M. Mitsuishi, "Virtual fixture assistance for suturing in robot-aided pediatric endoscopic surgery," *IEEE Robotics and Automation Letters*, vol. 5, no. 2, pp. 524–531, 2020.

[10] J. Abbott and A. Okamura, "Pseudo-admittance bilateral telemanipulation with guidance virtual fixtures," in *14th Symposium on Haptic Interfaces for Virtual Environment and Teleoperator Systems*, pp. 169–175, 2006.

[11] D. Shi, W. Zhang, W. Zhang, and X. Ding, "Assist-as-needed attitude control in three-dimensional space for robotic rehabilitation," *Mechanism and Machine Theory*, vol. 154, p. 104044, 2020.

[12] P. Agarwal and A. D. Deshpande, "Subject-specific assist-as-needed controllers for a hand exoskeleton for rehabilitation," *IEEE Robotics and Automation Letters*, vol. 3, no. 1, pp. 508–515, 2017.

[13] X. Jin, X. Cui, and S. K. Agrawal, "Design of a cable-driven active leg exoskeleton (c-alex) and gait training experiments with human subjects," in *2015 IEEE International Conference on Robotics and Automation (ICRA)*, pp. 5578–5583, IEEE, 2015.

[14] H. J. Asl, M. Yamashita, T. Narikiyo, and M. Kawanishi, "Field-based assist-as-needed control schemes for rehabilitation robots," *IEEE/ASME Transactions on Mechatronics*, vol. 25, no. 4, pp. 2100–2111, 2020.

[15] L. Pezeshki, H. Sadeghian, M. Keshmiri, X. Chen, and S. Haddadin, "Cooperative assist-as-needed control for robotic rehabilitation: A two-player game approach," *IEEE Robotics and Automation Letters*, vol. 8, no. 5, pp. 2852–2859, 2023.

[16] A. Duschau-Wicke, J. Von Zitzewitz, A. Caprez, L. Lunenburger, and R. Riener, "Path control: a method for patient-cooperative robot-aided gait rehabilitation," *IEEE transactions on neural systems and rehabilitation engineering*, vol. 18, no. 1, pp. 38–48, 2009.

[17] S. Kana, K.-P. Tee, and D. Campolo, "Human–robot co-manipulation during surface tooling: A general framework based on impedance control, haptic rendering and discrete geometry," *Robotics and Computer-Integrated Manufacturing*, vol. 67, p. 102033, 2021.

[18] H. J. Asl, T. Narikiyo, and M. Kawanishi, "An assist-as-needed velocity field control scheme for rehabilitation robots," in *2018 IEEE/RSJ International Conference on Intelligent Robots and Systems (IROS)*, pp. 3322–3327, 2018.

[19] H. J. Asl, T. Narikiyo, and M. Kawanishi, "An assist-as-needed control scheme for robot-assisted rehabilitation," in *2017 American control conference (ACC)*, pp. 198–203, IEEE, 2017.

[20] B. W. Gasser, A. Martínez, E. Sasso-Lance, C. Kandilakis, C. M. Durrough, and M. Goldfarb, "Preliminary assessment of a hand and arm exoskeleton for enabling bimanual tasks for individuals with hemiparesis," *IEEE Transactions on Neural Systems and Rehabilitation Engineering*, vol. 28, no. 10, pp. 2214–2223, 2020.

[21] J. C. Perry, J. Rosen, and S. Burns, "Upper-limb powered exoskeleton design," *IEEE/ASME Transactions on Mechatronics*, vol. 12, no. 4, pp. 408–417, 2007.

[22] J. Sun, Y. Shen, and J. Rosen, "Sensor reduction, estimation, and control of an upper-limb exoskeleton," *IEEE Robotics and Automation Letters*, vol. 6, no. 2, pp. 1012–1019, 2021.

[23] B. Kim and A. D. Deshpande, "An upper-body rehabilitation exoskeleton harmony with an anatomical shoulder mechanism: Design, modeling, control, and performance evaluation," *The International Journal of Robotics Research*, vol. 36, no. 4, pp. 414–435, 2017.

[24] A. Frisoli, A. Montagner, L. Borelli, F. Salsedo, and M. Bergamasco, "A force-feedback exoskeleton for upper-limb rehabilitation in virtual reality," *Applied Bionics and Biomechanics*, vol. 6, pp. 115–126, 2009.

[25] R. Shadmehr and F. Mussa-Ivaldi, "Adaptive representation of dynamics during learning of a motor task," *Journal of Neuroscience*, vol. 14, no. 5, pp. 3208–3224, 1994.

[26] T. Abuhamdia and J. Rosen, "Constant Visual and Haptic Time Delays in Simulated Bilateral Teleoperation: Quantifying the Human Operator Performance," *Presence: Teleoperators and Virtual Environments*, vol. 22, no. 4, pp. 271–290, 2013.

[27] A. Steed, S. Friston, V. Pawar, and D. Swapp, "Docking haptics: Extending the reach of haptics by dynamic combinations of grounded and worn devices," in *Proceedings of the 26th ACM Symposium on Virtual Reality Software and Technology*, VRST '20, (New York, NY, USA), Association for Computing Machinery, 2020.

[28] B. Maric, A. Mutka, and M. Orsag, "Collaborative human-robot framework for delicate sanding of complex shape surfaces," *IEEE Robotics and Automation Letters*, vol. 5, no. 2, pp. 2848–2855, 2020.

[29] J. E. Solanes, L. Gracia, P. Muñoz-Benavent, A. Esparza, J. Valls Miro, and J. Tornero, "Adaptive robust control and admittance control for contact-driven robotic surface conditioning," *Robotics and Computer-Integrated Manufacturing*, vol. 54, pp. 115–132, 2018.

[30] E. Todorov, T. Erez, and Y. Tassa, "Mujoco: A physics engine for model-based control," in *2012 IEEE/RSJ Int. Conf. on Intelligent Robots and Systems*, pp. 5026–5033, 2012.

[31] E. Rohmer, S. P. N. Singh, and M. Freese, "V-rep: A versatile and scalable robot simulation framework," in *2013 IEEE/RSJ International Conference on Intelligent Robots and Systems*, pp. 1321–1326, 2013.

[32] R. S. D'Souza and C. Nielsen, "An algorithm for local transverse feedback linearization," *SIAM Journal on Control and Optimization*, vol. 61, no. 3, pp. 1248–1272, 2023.

[33] R. J. Gill, D. Kulić, and C. Nielsen, "Spline path following for redundant mechanical systems," *IEEE Transactions on Robotics*, vol. 31, no. 6, pp. 1378–1392, 2015.

[34] J. Sun and R. Gill, "Vehicle platoon control with virtual path constraints," in *2019 IEEE Conference on Control Technology and Applications (CCTA)*, pp. 456–461, 2019.

[35] J. Sun, P. W. Ferguson, and J. Rosen, "Suppressing delay-induced oscillations in physical human-robot interaction with an upper-limb exoskeleton using rate-limiting," in *2022 IEEE/RSJ Int. Conf. on Intelligent Robots and Systems (IROS)*, pp. 6695–6701, 2022.

[36] F. Dimeas and N. Aspragathos, "Online stability in human-robot cooperation with admittance control," *IEEE Transactions on Haptics*, vol. 9, no. 2, pp. 267–278, 2016.

[37] F. Ferraguti, C. Talignani Landi, L. Sabattini, M. Bonfé, C. Fantuzzi, and C. Secchi, "A variable admittance control strategy for stable physical human–robot interaction," *The International Journal of Robotics Research*, vol. 38, 2019.

[38] A. Sharkawy, P. Koustoumpardis, and N. Aspragathos, "A neural network-based approach for variable admittance control in human–robot cooperation: online adjustment of the virtual inertia," *Intelligent Service Robotics*, 2020.

[39] A. Isidori, M. Thoma, E. D. Sontag, B. W. Dickinson, A. Fettweis, J. L. Massey, and J. W. Modestino, *Nonlinear Control Systems*. Berlin, Heidelberg: Springer-Verlag, 3rd ed., 1995.

[40] Y. Shen, J. Sun, J. Ma, and J. Rosen, "Admittance control scheme comparison of exo-ul8: A dual-arm exoskeleton robotic system," in *IEEE 16th Int. Conf. on Rehabilitation Robotics (ICORR)*, pp. 611–617, 2019.

[41] R. M. Murray, Z. Li, and S. Sastry, *A Mathematical Introduction to Robotic Manipulation*. CRC Press, 1994.

[42] H. Martiros, A. Miller, N. Bucki, B. Solliday, R. Kennedy, J. Zhu, T. Dang, D. Pattison, H. Zheng, T. Tomic, P. Henry, G. Cross, J. Vander-Mey, A. Sun, S. Wang, and K. Holtz, "SymForce: Symbolic Computation and Code Generation for Robotics," in *Proceedings of Robotics: Science and Systems*, 2022.

[43] A. Meurer, C. P. Smith, M. Paprocki, O. Čertík, S. B. Kirpichev, M. Rocklin, A. Kumar, S. Ivanov, J. K. Moore, S. Singh, T. Rathnayake, S. Vig, B. E. Granger, R. P. Muller, F. Bonazzi, H. Gupta, S. Vats, F. Johansson, F. Pedregosa, M. J. Curry, A. R. Terrel, v. Roučka, A. Saboo, I. Fernando, S. Kulal, R. Cimrman, and A. Scopatz, "Sympy: symbolic computing in python," *PeerJ Computer Science*, vol. 3, p. e103, Jan. 2017.

Jianwei Sun received a B.Sc. in Engineering Science (1T6 + PEY) from the University of Toronto in 2017, a M.Sc. in Electrical Engineering and Information Technology from ETH Zürich in 2019, and a Ph.D. in Mechanical Engineering (Bionics Lab) from the University of California, Los Angeles (UCLA) in 2024. His research focuses on nonlinear control, estimation, and safety for physical human-robot interaction with exoskeletons and haptic robots.

Yasamin Foroutani received a B.Sc. in Mechanical Engineering from Sharif University of Technology in 2019. She is currently a Ph.D. candidate in the Department of Mechanical and Aerospace Engineering at the University of California, Los Angeles (UCLA), where she received a M.Sc. degree in 2022. Her research focuses on robot motion planning and image-based automation in surgical and haptic robots.

Jacob Rosen received a B.Sc. degree in mechanical engineering, and M.Sc. and Ph.D. degrees in biomedical engineering from Tel-Aviv University, Tel-Aviv, Israel, in 1987, 1993, and 1997, respectively. He is a professor in the Department of Mechanical and Aerospace Engineering and the director of the Bionics Lab at the University of California, Los Angeles (UCLA). His research interests focus on medical robotics, biorobotics, human-centered robotics, surgical robotics, wearable robotics, rehabilitation robotics, and neural control.